Received: 13 November 2023 | Revised: 19 July 2024 | Accepted: 27 August 2024

DOI: 10.1002/nme.7600

RESEARCH ARTICLE

WILEY

Reinforcement topology optimization considering the dynamic instability

Sol Ji Han | **Gil Ho Yoon**

School of Mechanical Engineering, Hanyang University, Seoul, South Korea

Correspondence
Gil Ho Yoon, School of Mechanical Engineering, Hanyang University, Seoul, South Korea.
Email: gilho.yoon@gmail.com

Funding information
Korea government (MSIT), Grant/Award Number: RS-2024-00351611

Abstract

The present study develops a new topology optimization scheme considering the dynamic instability caused by the unsymmetrical properties of system. From a mathematical point of view, the left and right eigenvectors of asymmetric system are observed with the complex eigenvalues. With the dynamic instability, the magnitudes of structural responses are increasing with respect to time and this phenomenon causes many engineering issues. As the dynamic instability is one of the serious problems, the suppression is desired from an engineering point of view. To systematically reduce this dynamic instability, the present study develops a new topology optimization scheme for the reinforcement design. To overcome the numerical difficulties of the mode conversion and the highly nonlinear behavior, this research proposes the summation of the first several complex eigenvalues. To show the issues of the dynamic instability and the validity of the present approach, several topological reinforcement problems are solved.

KEYWORDS

dynamic instability, reinforcement design, squeal noise, topology optimization

1 | INTRODUCTION

The present study develops a new topology optimization scheme considering the dynamic instability caused by the unsymmetrical properties of system. Particularly, the asymmetric system caused by the friction as shown in Figure 1 is considered. From a mathematical point of view, the left and right eigenvectors of asymmetric system are observed with the complex eigenvalues. With the dynamic instability, the magnitudes of structural responses are increasing with respect to time and this phenomenon causes many engineering issues. As the dynamic instability is one of the serious problems, the suppression is desired. To systematically reduce this dynamic instability, the present study develops a new topology optimization scheme for the reinforcement design. To overcome the numerical difficulties of the mode conversion and the highly nonlinear behavior, this research proposes the summation of the first several complex eigenvalues. To show the issues of the dynamic instability and the validity of the present approach, several topological reinforcement problems are solved.

Research on analyzing dynamic instability has been actively conducted in the field of engineering. The analysis related to squeal noise can be divided in terms of the analysis type, that is, time-transient analysis or complex eigenvalue analysis.[1,2] Complex eigenvalue analysis can further be divided into the analysis of static steady-sliding equilibrium and the stability analysis with rotation.[3] To analyze a brake system with friction through time-transient analysis, several studies have been conducted. In Reference 4, transient models of railway wheel noise were considered using axisymmetric decomposition in Fourier series. In Reference 5, transient nonlinear time-domain analysis has been employed to analyze

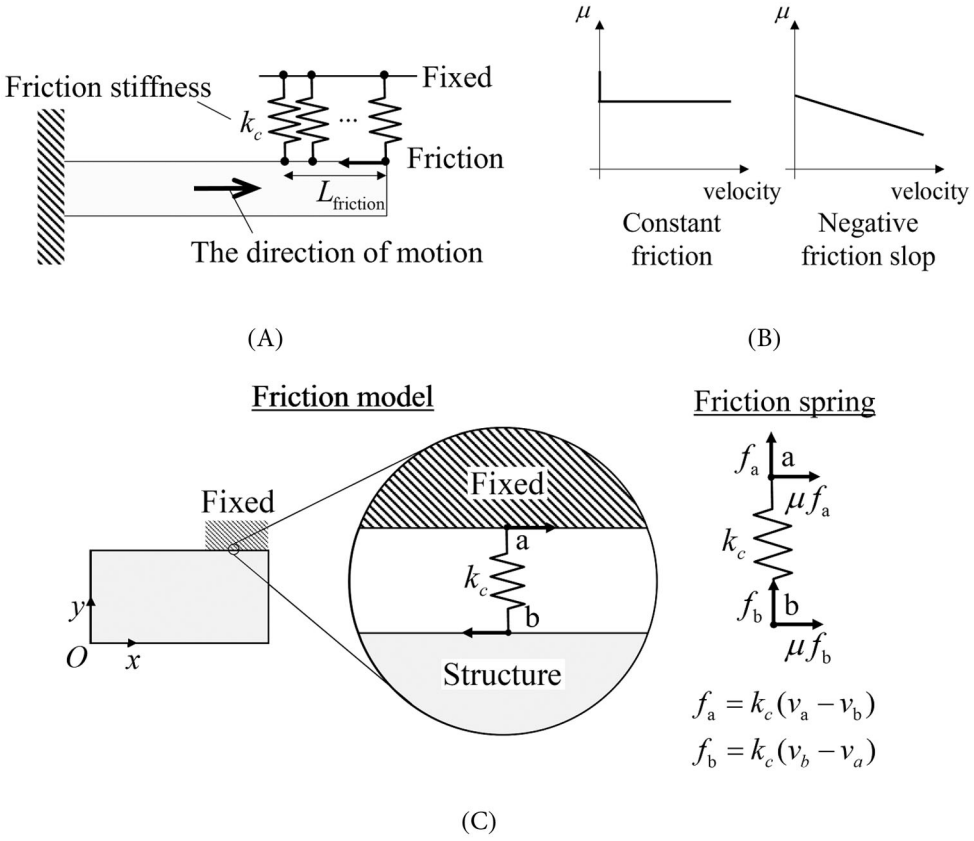

FIGURE 1 (A) Friction coefficients and the friction force and (B) the spring model for friction.

chaotic pad and disc motion. In Reference 6, complex eigenvalue analysis and dynamic transient analysis were performed to evaluate several friction material specimens in a pad-on-disk friction system. Additionally, several studies have investigated the stability analysis with rotation. In Reference 7, research has been conducted on the stability analysis of disc brakes, considering gyroscopic effects, negative friction slope, and mode-coupling. In Reference 8, the study has been done on the nonlinear stability analysis of a disk brake model consisting of 12 degrees of freedom. In Reference 9, the dynamic instability analysis by rotation effect is considered. Furthermore, to analyze dynamic instability through complex eigenvalue analysis of static steady-sliding equilibrium, several methods have been developed. In Reference 10, to estimate the squeal of disc brake, complex eigenvalue analysis and design of experiments were carried out. In Reference 11, nonlinear analysis was employed for complex eigenvalue analysis related to the stability of brake system using Abaqus/standard. In Reference 12, finite element modeling concerning the squeal propensity of in-plane modes and the role of damping shims in disc brake squeal was employed. Moreover, studies have been carried out to analyze brake systems more accurately, addressing factors such as friction springs,[13,14] structural damping,[15] gyroscopic effects,[16,17] and the negative slope of friction.[18]

To mitigate the dynamic instability, the structural optimization scheme can be applied. In Reference,[19] the focus was on sensitivity analysis for reducing dynamic instability. In Reference 20, nonparametric shape optimization was employed to suppress dynamic instability. In Reference 21, a combination of FE transient dynamic analysis, Kriging surrogate modeling, and size optimization techniques was presented to minimize squeal instability in multi-variable squeal problems. In the field of topology optimization for eigenvalue problems, several methods have been developed for the frequency domain. In Reference 22, an approach was presented to facilitate sensitivity analysis for repeated eigenvalues. In Reference 23, numerical examples are presented to demonstrate the maximization of the first eigenfrequency while avoiding localized modes in low-density areas. However, there has been limited topology optimization aimed at reducing dynamic instability in complex eigenvalue problems.

The remainder of this article is organized as follows. Section 2 provides the basic concept of the friction spring and its model in addition to the mathematical formula. The difficulties in considering the friction in topology optimization are discussed and the necessity of the reinforcement formulation is discussed. The optimization formulation emphasizing

the type of the objective function and its sensitivity analysis are presented. Section 3 describes several topology optimization examples that show the properties of the friction in the structural topology optimization. Section 4 presents the conclusions of the study and provides suggestions for future research.

2 | DYNAMIC INSTABILITY AND TOPOLOGY OPTIMIZATION FORMULATION

2.1 | Dynamic instability

The present study considers the dynamic instability caused by asymmetric system matrix. One of the representative examples may be the phenomenon called the squeal noise as shown in Figures 1 and 2. From the perspective of the brake

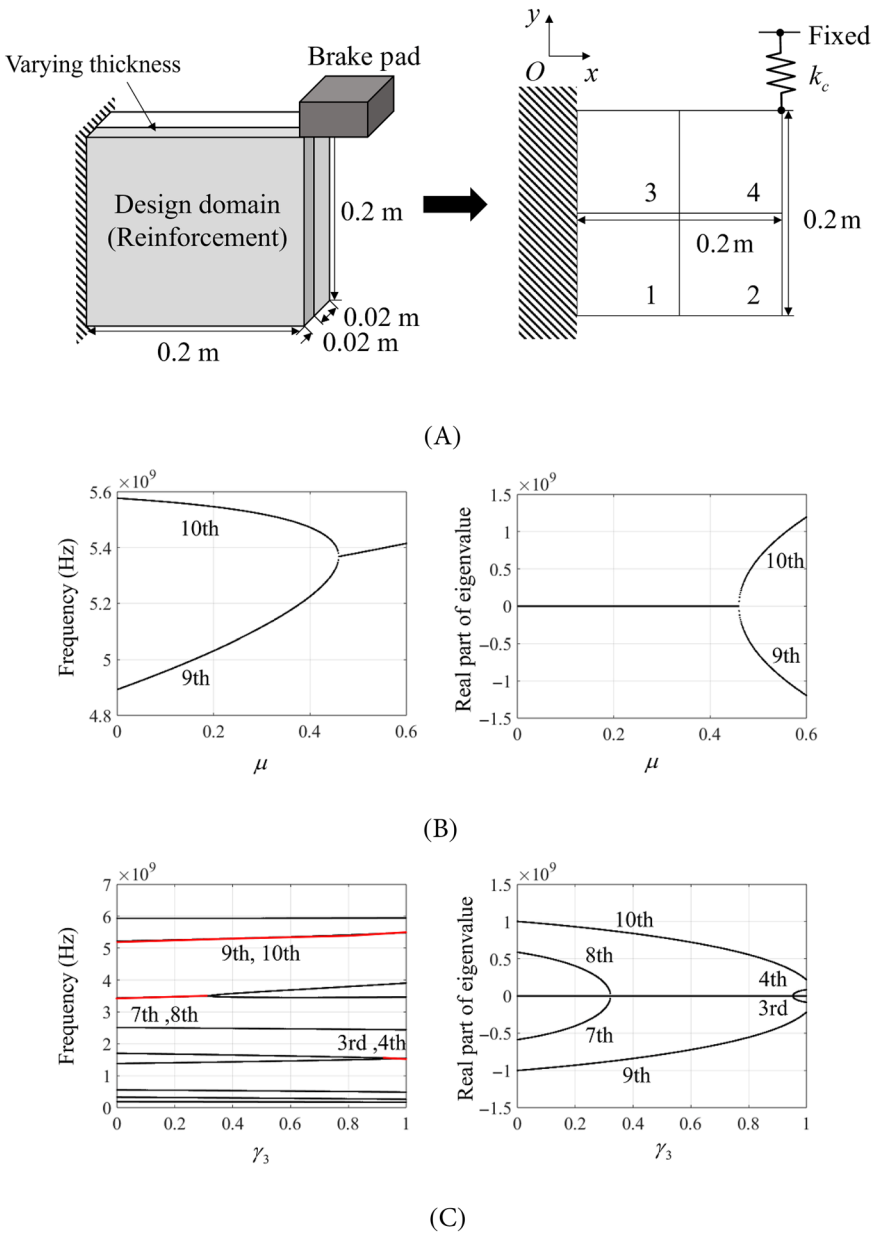

FIGURE 2 An element two by two quad example. (A) the problem with four quad elements (Young's modulus = 200 GPa, $\rho = 7800$ kg/m^3, $\nu = 0.3$, $k_c = 10^{14}$ N/m, $\mu = 0.5$, mass and stiffness penalization factors = 1, initial density = 0.3), (B) the mode coupling with the various friction coefficient and (C) the mode coupling with the various density of the first element.

friction modeling, it can be described either by a constant value or a negative slope shown in Figure 1. With a nonzero relative velocity between contact surfaces, the friction coefficient either is constant or is varied. In this study, the modeling with a constant friction coefficient is utilized for the illustrative purpose. The drawing the free body diagram with the constant friction coefficient results in the friction spring model with the asymmetric friction stiffness matrix. Figure 2 illustrates the perplex behavior of the brake friction system on a reinforcement plate. By increasing the friction coefficient μ from 0 to 0.6, the mode coupling phenomenon becomes serious. In addition, the variation of the density of the first element between zero and one causes the dynamic instability too. These two illustrative examples show the typical issues encountered in the optimization of the dynamic instability. The phenomenon called squeal noise refers a dynamic instability caused by stick-slip, sprag-slip, or mode coupling between objects contacting each other.[24] The stick-slip instability occurs due to the difference of the static coefficient of friction and the dynamic coefficient of friction. The sprag-slip instability refers the instability due to the geometric and the kinematic constraints. The instability due to the mode coupling occurs when the eigenmodes of disk, pad, or calipers are coupled. The mode coupling refers a phenomenon in which two imaginary eigenvalues approach each other and merge into a single value by frictional force. The real parts of the eigenvalues appear with opposite signs and equal magnitudes in the absence of damping. In addition, there are studies on squeal with nonlinear behavior. In Reference 25, the nonlinear distribution of the friction coefficient and friction force was studied. In this article, we only apply the linear distribution of friction force. To our best knowledge, few research exists for the topology optimization with the structural instability. It is our findings that the oscillation of the problematic eigenmodes with positive real values makes the topology optimization difficult and challenging. Especially, the eigenmodes with nonzero real values are newly considered in the present study.

With an asymmetric system matrix, complex eigenvalue values are obtained. With positive values in the real parts of the complex eigenvalues, the corresponding system becomes unstable.[26,27] Therefore, the goal of this study is to mitigate the dynamic instability by decreasing or removing the positive values of complex eigenvalues. Without the loss of generality, the eigenvalue problem of asymmetric matrix can be formulated as follows:

$$\left(\mathbf{K} + \lambda_i^2 \mathbf{M}\right)\Phi_{ri} = \mathbf{0}, \tag{1}$$

$$\Phi_{li}^{\mathrm{T}}\left(\mathbf{K} + \lambda_i^2 \mathbf{M}\right) = \mathbf{0}, \tag{2}$$

where the ith right eigenvectors and the ith left eigenvectors are denoted by Φ_{ri} and Φ_{li}, respectively. The ith eigenvalue is denoted by λ_i. Note that for symmetric system, the eigenvalues are pure imaginary values and the right and left eigenvectors are identical. However, the complex eigenvalues should be considered and the left and the right-side eigenvectors should be considered for asymmetric system. Considering the dynamic instability, the above two eigenvectors are not identical and should be computed separately.

In the asymmetric system with the dynamic instability, not only the eigenvectors (Φ_{ri} and Φ_{li}) but also the eigenvalues (λ_i) are complex.[28] The behavior of the structural response with respect to time is mainly governed by the magnitude of the real parts of the complex eigenvalues. Therefore, it has been one of the important engineering problems to reduce the structural instability considering the magnitude of the squeal noise or the shapes of the complex eigenvectors.[29–32]

2.2 | Topology optimization formulation considering the dynamic instability

The considering of the eigenvalue in topology optimization is challenging due to the highly nonlinear behavior, the mode coupling and the mode switching (See the Appendix A). To consider these challenging issues rigorously, this research presents the usage of the *summation* of the first *Neigen* eigenfrequencies based on the *reinforcement design formulation* as follows:

$$\begin{aligned} &\underset{\gamma_e}{\mathrm{Min}} \sum_{i=1}^{\mathrm{Neigen}} \mathrm{real}(\lambda_i)^2 \\ &\text{Subject to } V(\gamma_e) \le V_0 \\ &\qquad (\mathbf{K} + \lambda_i^2 \mathbf{M})\Phi_{ri} = \mathbf{0}, 0 \le \gamma_e \le 1, \end{aligned} \tag{3}$$

where the design variables are denoted by γ_e. The sum of the real parts of all the first Neigen eigenvalues, λ_i, $i = 1, 2, \ldots, \mathrm{Neigen}$, are considered as the objective function. The volume, $V(\gamma_e)$, is constrained with the upper bound, V_0.

The stiffness and the mass matrices are denoted by **K** and **M**, respectively. The right eigenvectors associated with the eigenvalues λ_i are denoted by Φ_{ri}. Rather than the sum of the square of the real values of the complex eigenvalues, it is also possible to set the objective domain with the pseudo maximum value or the *p*-norm of the real values of the complex eigenvalues. To avoid the local mode issue and the highly nonlinear behavior of the complex eigenvalue (Refer the Appendix A for more detail), the reinforcement formulation is set as follows:

$$\mathbf{K} = \sum_{e=1}^{ne} (\gamma_e t_1 + t_2)\mathbf{K}_0, \ \mathbf{M} = \sum_{e=1}^{ne} (\gamma_e t_1 + t_2)\mathbf{M}_0, \tag{4}$$

where the total number of elements is denoted by *ne* and the basic stiffness and mass matrices of the plane stress element are denoted by $\mathbf{K}_0$ and $\mathbf{M}_0$, respectively. In the present study, the four node finite element is utilized and refer the finite element book for the formulation and implementation. Not presented here but our trials to solve the topology optimization with void and solid turn out failures due to the complex behaviors of the objective function. Compared with the topology optimization problem with void or solid, the above reinforcement design makes the highly nonlinear behavior of topology optimization relax to be solved by a gradient-based optimization process. The basic thickness is denoted by t_2 and the thickness of the reinforcement structure is denoted by t_1. Normally, the reinforcement thickness is smaller than the basic thickness to prevent too significant ruptures in the behavior of a considered mechanical system. The *e*th design variable is denoted by γ_e. The design variable which represents the reinforcement thickness is varied from zero to one. The sensitivity of the objective function can be formulated as follows:

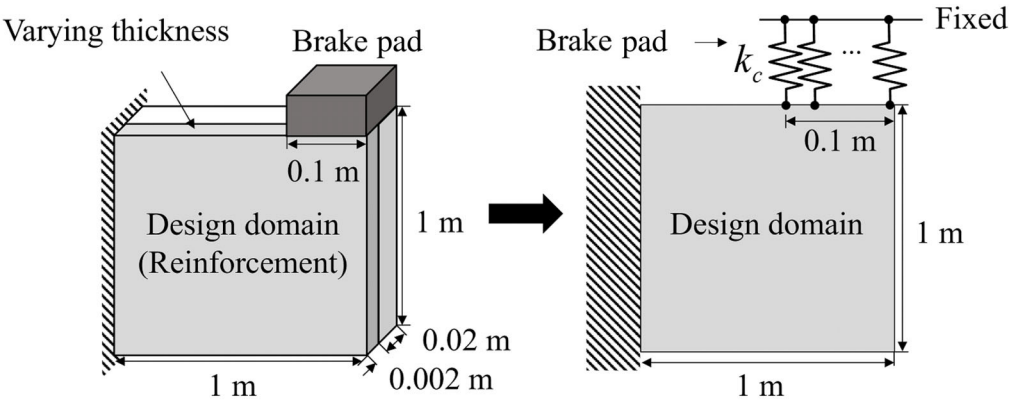

(A)

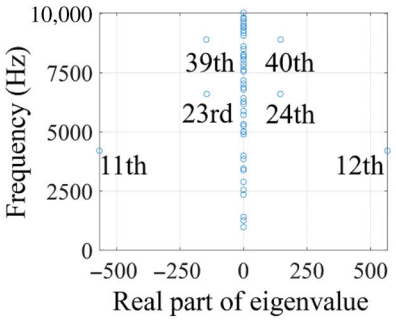

Complex eigenvalue with nonzero real part

i	Real (λ_i) (rad/s)	Imag (λ_i) (rad/s) / Frequency (Hz)
11	−567.01 (rad/s)	28,306 (rad/s) / 4205.1 (Hz)
12	567.01 (rad/s)	28,306 (rad/s) / 4205.1 (Hz)
23	−145.05 (rad/s)	41,489 (rad/s) / 6603.1 (Hz)
24	145.05 (rad/s)	41,489 (rad/s) / 6603.1 (Hz)
39	−146.35 (rad/s)	55,918 (rad/s) / 8899.6 (Hz)
40	146.35 (rad/s)	55,918 (rad/s) / 8899.6 (Hz)

(B)

FIGURE 3 Example 1: (A) the problem of reinforcement in-plane elements (the number of elements: 50 by 50, Young's modulus = 200 GPa, $\rho = 7800$ kg/m^3, $\nu = 0.3$, the mass and stiffness penalizations = 1, the number of friction spring: 6, $\mu = 0.5$) and (B) the eigenvalue analysis of the initial model with the three real complex values (Initial density=0.5).

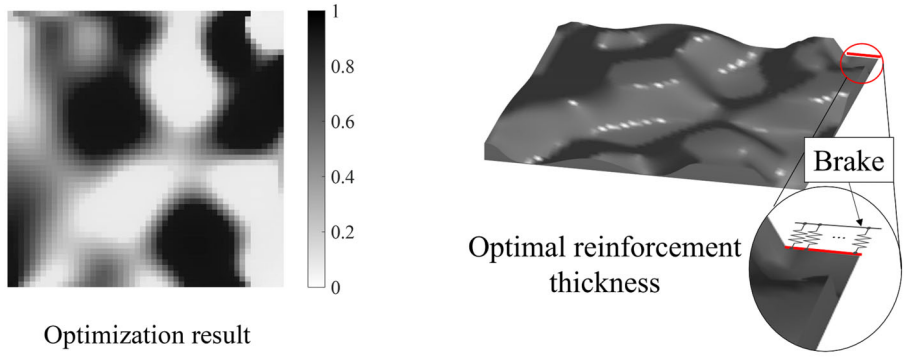

(A)

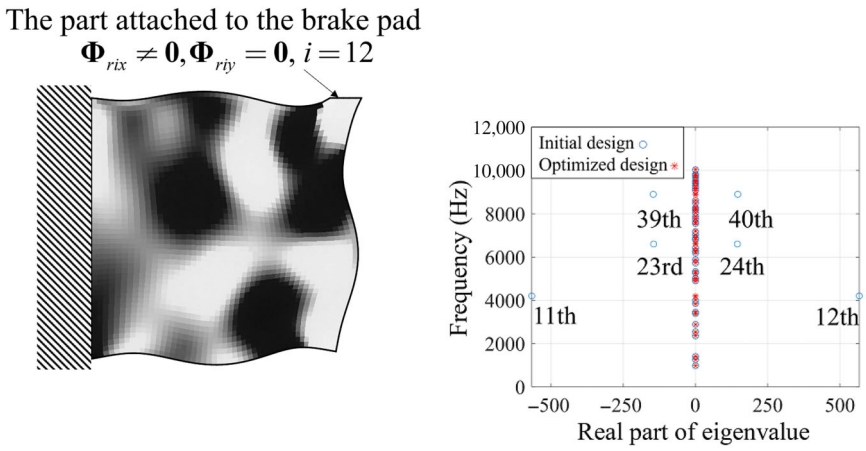

(B) (C)

FIGURE 4 (A) An optimized layout with the first 50 eigenvalues (left: the design variable distribution and right: 3d plot), (B) the 12th eigenvector (Φ_{rix}: the x-direction component of the eigenvector, Φ_{riy}: the y-direction component of the eigenvector) and (C) the distributions of the eigenvalues.

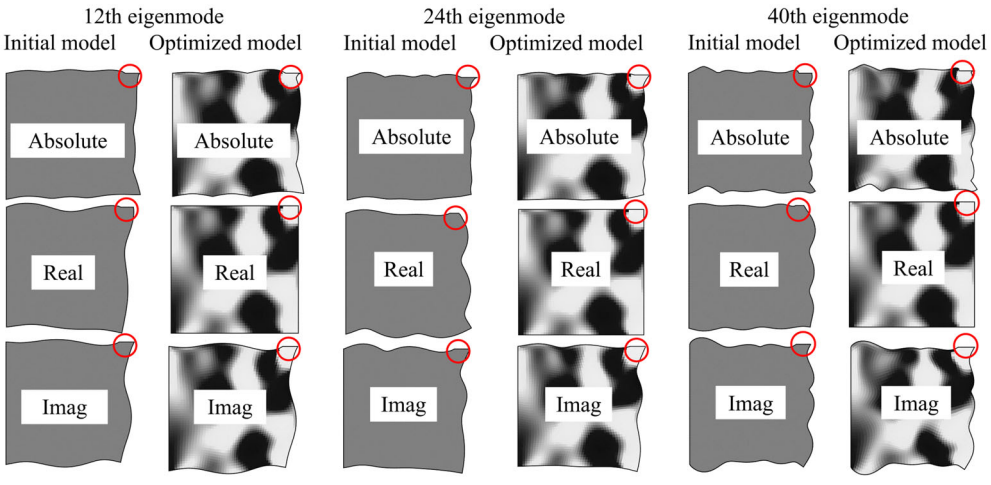

(A) (B) (C)

FIGURE 5 (A–C) The right eigen mode shapes of the 12th, the 24th and the 40th eigenmodes, respectively (the eigenvectors near the brake are marked by the red circles.). (Due to the conjugate eigenvalues, the eigenmodes of the 11th, the 23rd and the 39th modes are same as those of the 12th, the 24th and the 40th modes.)

$$\frac{\partial}{\partial \gamma_e}\sum_{i=1}^{\text{Neigen}} \text{real}(\lambda_i)^2 = \sum_{i=1}^{\text{Neigen}} 2\ \text{real}(\lambda_i)\text{real}\left(\frac{\partial \lambda_i}{\partial \gamma_e}\right), \tag{5}$$

$$\begin{aligned}\left(\frac{\partial \mathbf{K}}{\partial \gamma_e} + 2\lambda_i \frac{\partial \omega}{\partial \gamma_e}\mathbf{M} + \lambda_i^2 \frac{\partial \mathbf{M}}{\partial \gamma_e}\right)\Phi_{ri} + \left(\mathbf{K} + \lambda_i^2 \mathbf{M}\right)\frac{\partial \Phi_{ri}}{\partial \gamma_e} = \mathbf{0} \\ \Phi_{li}^{\mathrm{T}}\left(\frac{\partial \mathbf{K}}{\partial \gamma_e} + 2\lambda_i \frac{\partial \lambda_i}{\partial \gamma_e}\mathbf{M} + \lambda_i^2 \frac{\partial \mathbf{M}}{\partial \gamma_e}\right)\Phi_{ri} = \mathbf{0},\end{aligned} \tag{6}$$

$$\frac{\partial \lambda_i}{\partial \gamma_e} = -\frac{\Phi_{li}^{\mathrm{T}}\left(\frac{\partial \mathbf{K}}{\partial \gamma_e} + \lambda_i^2 \frac{\partial \mathbf{M}}{\partial \gamma_e}\right)\Phi_{ri}}{2\lambda_i \Phi_{li}^{\mathrm{T}} \mathbf{M} \Phi_{ri}}, \frac{\partial \mathbf{K}}{\partial \gamma_e} = t_1 \mathbf{K}_0, \frac{\partial \mathbf{M}}{\partial \gamma_e} = t_1 \mathbf{M}_0. \tag{7}$$

The sensitivity analysis of the real part of the complex eigenvalues can be found in some relevant papers.[20] This study proposes to sum several eigenvalues to overcome the side effect of the mode switching and the highly nonlinear behaviors of the real parts of the eigenvalues with respect to the design variables. Alternatively, the p-norm value of the eigenvalues can be set as the objective function as follows:

$$\begin{aligned}&\underset{\gamma_e}{\text{Min}}\left(\sum_{i=1}^{\text{Neigen}} \text{real}(\lambda_i)^p\right)^{1/p} \\ &\text{Subject to } V(\gamma_e) \le V_0 \\ &\qquad (\mathbf{K} + \lambda_i^2 \mathbf{M})\Phi_{ri} = \mathbf{0}.\end{aligned} \tag{8}$$

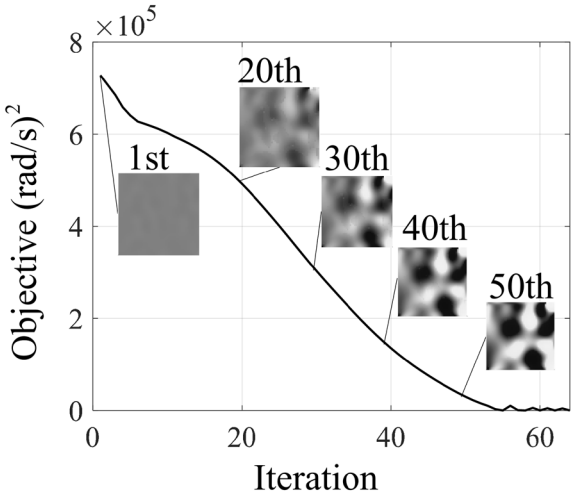

(A)

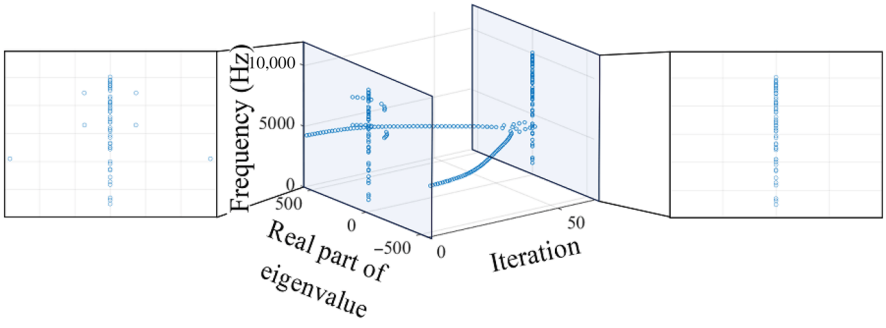

(B)

FIGURE 6 (A) The optimization convergence and (B) the evolution of the complex eigenvalues during the optimization.

It is also beneficial by smoothing the objective function when some real parts vanish that causes the oscillations with objective or constraint functions formulated with one or a few real values of eigenvalues. Considering the results of our study, this p-norm in the objective is also beneficial to reduce the side effect of the mesh refinement and the initial condition. The sensitivity of the p-norm foam can be derived as follows:

$$\frac{\partial\left(\sum_{i=1}^{\text{Neigen}}\text{real}(\lambda_i)^p\right)^{1/p}}{\partial\gamma_e}=\left(\sum_{i=1}^{\text{Neigen}}\text{real}(\lambda_i)^p\right)^{(1-p)/p}\times\sum_{i=1}^{\text{Neigen}}\text{real}(\lambda_i)^{p-1}\text{real}\left(\frac{\partial\lambda_i}{\partial\gamma_e}\right). \tag{9}$$

3 | NUMERICAL EXAMPLES

To demonstrate the practical application of the current topology optimization approach, we tackle multiple optimization problems pertaining to the dynamic instability causing squeal noise in a two-dimensional model. We employ the optimization algorithm (MMA)[33] to solve the ensuing optimization formulation.

3.1 | Example 1: Topology optimization for reinforcement design for unit square plate

For the first optimization example, we consider the topology optimization problem employing in-plane elements with reinforcement in the square geometry in Figure 3A. A brake pad is positioned at the upper right corner of the disk, while

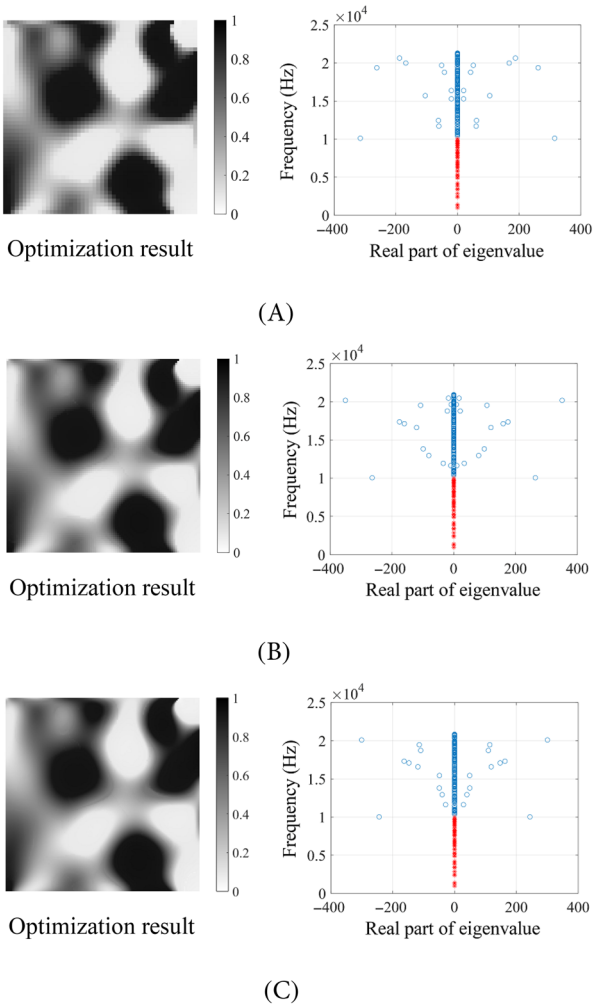

FIGURE 7 The effect of the mesh refinement. (A) a 50 by 50 elements with 6 springs, (B) a 100 by 100 elements with 11 springs and (C) 150 by 150 elements with 16 springs (Red circles: the first 50 eigenvalues and blue circles: the rest eigenvalues).

the fixed supports are defined along the left side. The first 50 complex eigenvalues are listed in Figure 3B. With the given initial design (Initial density: 0.5), the 12th, 24th, and 40th eigenvalues have positive real values that cause the dynamic instability. To minimize the real values of the complex eigenvalues, the sum of squares of the 50 real parts of eigenvalues is set to the objective function.

To minimize the dynamic instability caused by these complex eigenvalues with nonzero real parts, it is possible to design a reinforcement structure by topology optimization. With the present optimization formulation with the first 50 eigenvalues, the optimized reinforcement design in Figure 4 can be obtained. Figure 4A shows the distribution of the reinforcement thickness. The first investigation of the optimized layout reveals that some reinforcement structure appears near the area contacting with the springs simulating a brake. By investigating the eigenmodes in Figures 4B and 5, it is our finding that the presented topology optimization scheme finds out an optimized reinforcement thickness to make the value of the eigenvalue in the y-direction zero or almost zero (See the red circles in Figure 5). From a mathematical point of view, it does make sense as the force exerted by the brake springs is modeled to be proportional to the vertical deformation. Therefore, the topology optimization scheme tries to minimize the eigenmode shape in the y-direction near the area with the brake springs by increasing the stiffness by the reinforcement. By this reinforcement optimization process, the three troublesome modes can be successfully suppressed or the three eigenmodes become higher modes as shown in Figure 4C.

Figure 6 shows the optimization history and the evolution of the complex eigenmodes during the optimization history. The investigation of the optimization history shows that the presented objective function, that is, the summation of the squares of the eigenvalues, can be smoothly decreased during the optimization process. The evolution of the complex eigenvalues in Figure 6B shows that the magnitudes of the 11th and 12th complex eigenvalues are decreasing by the topology optimization and some oscillations occur at the end of the optimization process due to (1) the oscillations of

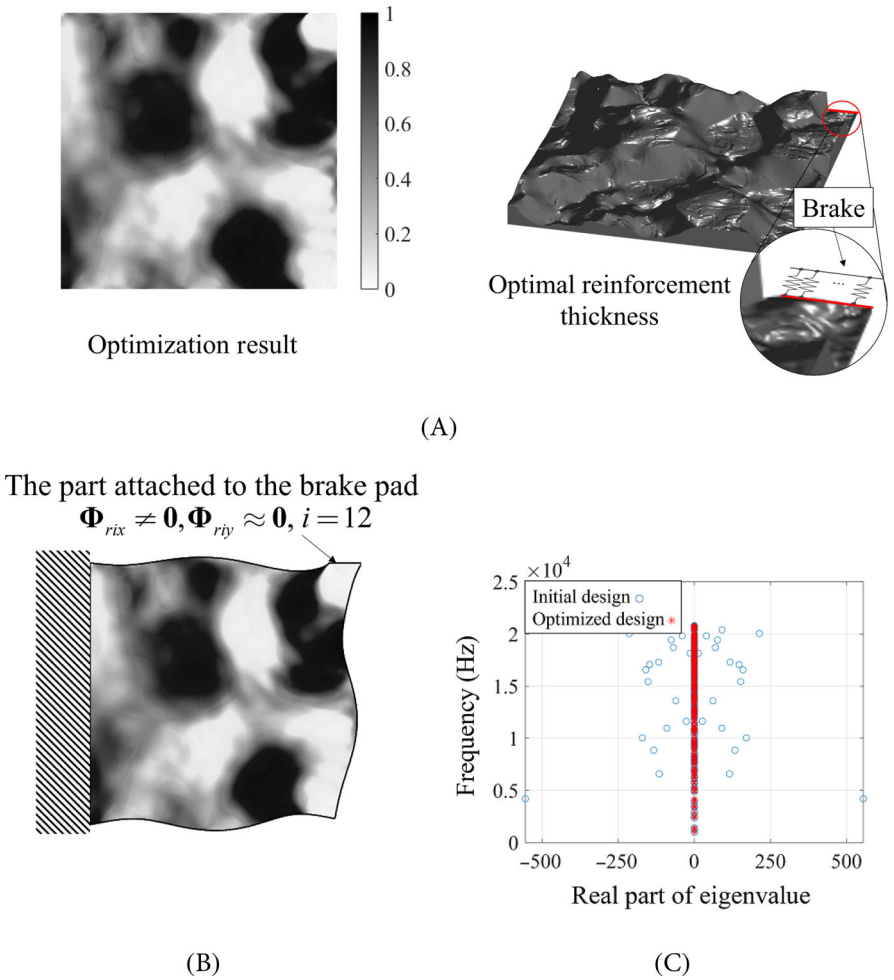

FIGURE 8 Example 1: (A) an optimized layout with 200 eigenvalues (the number of elements: 300 by 300, the number of friction spring: (31), (B) the eigenmode of the largest real eigenmode, and (C) the eigenvalue distribution.

the complex eigenvalues and (2) the mode switching of the eigenvalues. This example shows that the present scheme can successfully suppress the complex eigenvalue issue and the dynamic instability issue in engineering. To our best knowledge, the findings in this research are the first in the world from a structural optimization point of view.

The mesh refinement is one of the important aspects in the optimization of the dynamic instability. To our experience, unlike static or simple eigenvalue problems, the complex eigenvalue problem of the dynamic instability requires tailored meshes. Figure 7A shows the distribution of the 200 complex eigenvalues. Several refined meshes and their solutions are computed and compared. It is also confirmed that with the refined meshes, the optimized layouts are also similar to each others. We can see that while the overall layouts are similar, the distributions of the eigenvalues are different. Nevertheless, all the first 50 eigenvalues of the three designs do not contain real parts, indicating that the systems are stable from a dynamic stability point of view.

Then Figure 8 investigates the number of the complex eigenvalues in the objective function. For an example, the objective function with the first 200 eigenvalues is considered. The overall layout is similar to the layout with the first 50 eigenvalues. However, some random distributions of the reinforcement can be found. We postulate that this is due to the effect of the higher complex eigenvalues whose eigenvectors are localized compared with the eigenvectors of the low complex eigenvalues. Figure 9 shows the optimization history and the convergence of the complex eigenvalues. As observed in Figure 9, the stable convergence can be obtained. However, some bumps are observed due to (1) the oscillations of the complex eigenvalues and (2) the mode switching of the eigenvalues.

In the optimization, it is also possible to consider the p-norm for the objective function. To our numerical test in Figure 10, we observed that the overall procedure is similar with the two-norm. This example shows that by considering the different setting of the complex eigenvalues, it is possible to control the distributions of the complex eigenvalues. As illustrated in the figure of the real and imaginary values during an optimization process, the adoption of the p-norm in the objective function allows to reduce the real parts of eigenvalues smoothly.

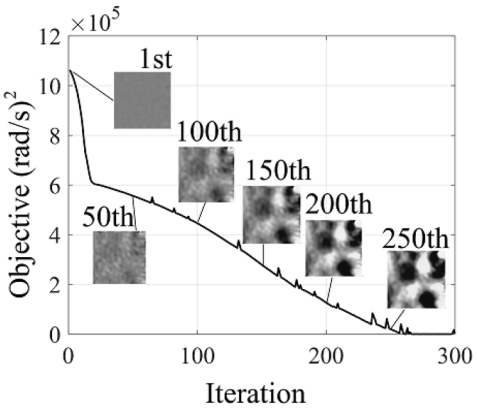

(A)

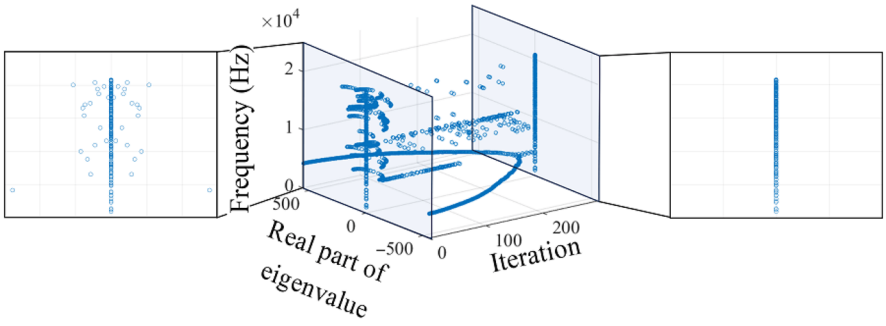

(B)

FIGURE 9 (A) The optimization history of sum for square real eigenvalue and (B) the evolution of the complex eigenvalues during the optimization.

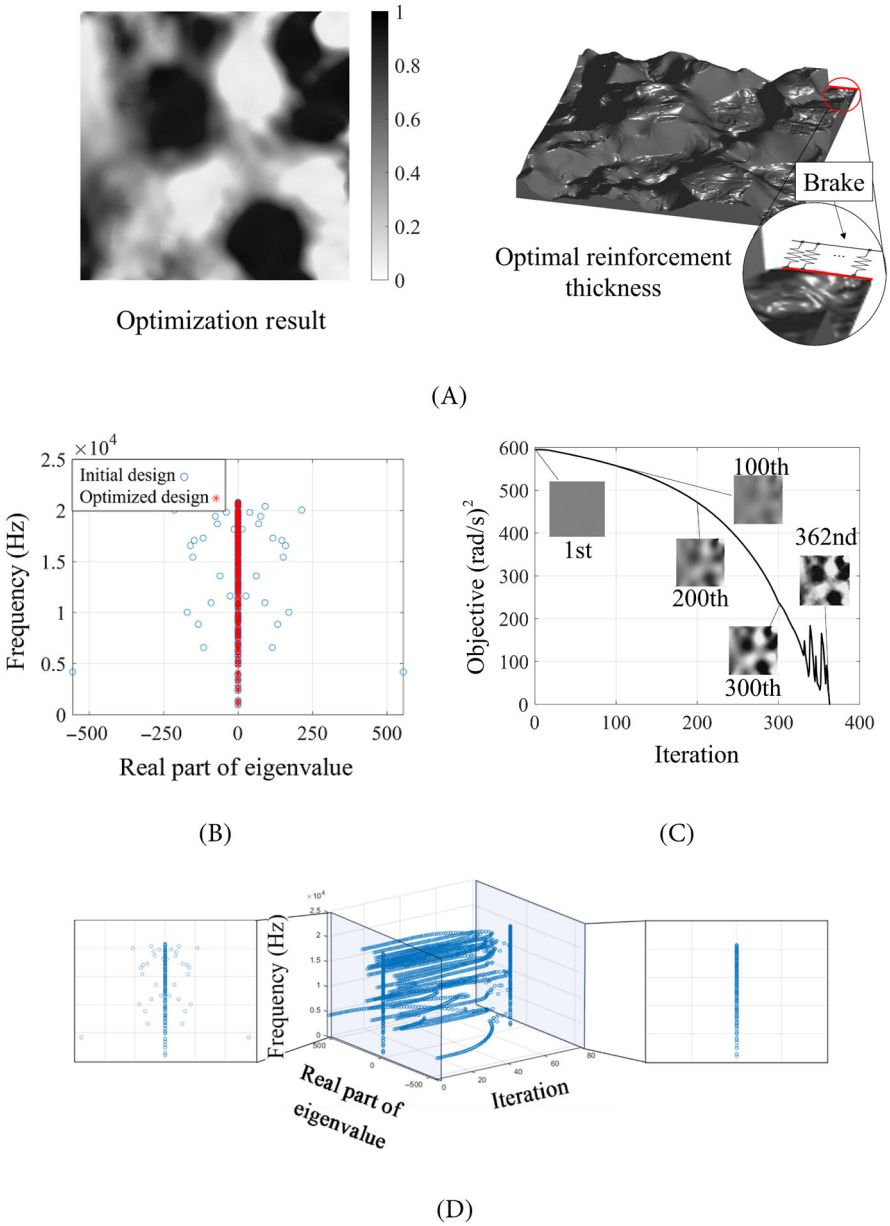

FIGURE 10 (A) The density optimization result with the first 200 eigenvalues using the p-norm (the size of elements = 300 by 300, the number of friction spring: 31, $p = 10$), (B) the eigenvalue distribution, and (C) the optimization history, and (D) the evolution of the complex eigenvalues during the optimization.

3.2 | Example 2: Topology optimization for reinforcement design

For the next example showing the validity of the present scheme, the topology optimization example in Figure 11 is considered. As in the first example, the reinforcement design is considered. The material properties for structure and brake are set as the first example. In this example, the two complex eigenvalues are observed at the 21st and the 22nd modes. Figure 12A shows the distribution of the optimized thickness. As observed in the first example, to minimize the effect of the dynamic instability, the complex values of the associated eigenmodes become real values an the eigenmodes in the y-direction near at the brake become near zeros. In addition, to increase the eigenvalues, the reinforcement thicknesses are optimized. Figure 13 shows the optimization history.

To investigate the effect of the brake location, Figure 14 considers the topology optimization problem with a center brake. In this configuration, the four complex eigenvalues are observed. Figures 15 and 16 show the optimized layout and the optimization history. This example also shows that the present approach becomes one of the engineering tools to consider the dynamic instability.

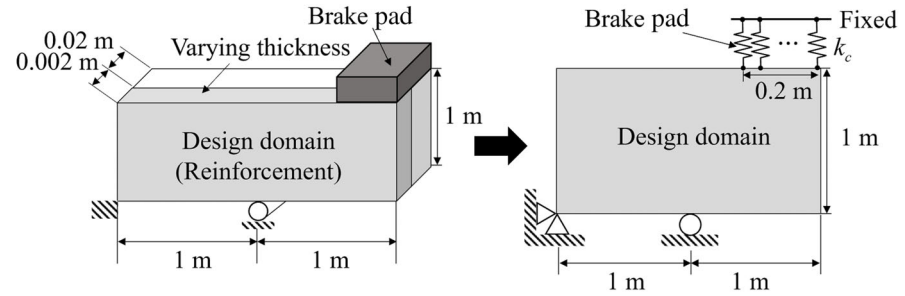

(A)

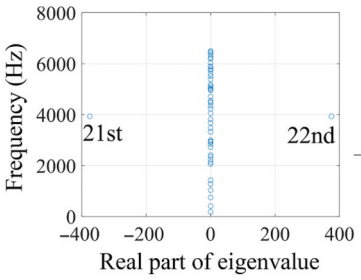

Complex eigenvalue with nonzero real part

i	Real (λ_i) (rad/s)	Imag (λ_i) (rad/s) / Frequency (Hz)
21	−374.96 (rad/s)	24,722 (rad/s) / 3934.7 (Hz)
22	374.96(rad/s)	24,722 (rad/s) / 3934.7 (Hz)

(B)

FIGURE 11 Example 2-1: (A) the reinforcement problem with a disk pad (the number of elements: 200 by 100, Young's modulus = 200 GPa, $\rho = 7800$ kg/m^3, $\nu = 0.3$, the mass and stiffness penalization factors = 1, the number of friction spring: 21, $\mu = 0.5$) and (B) the eigenvalue analysis of the initial model with the two real complex values (Initial density = 0.5).

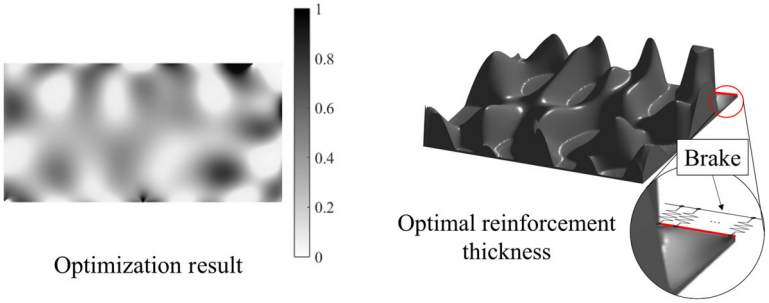

(A)

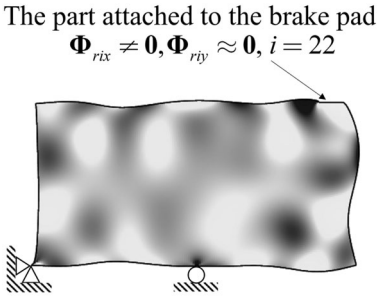

(B)

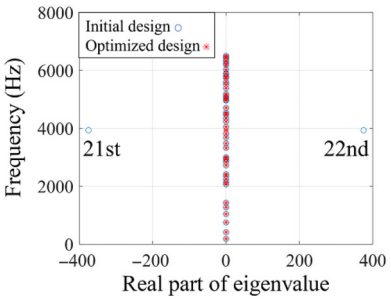

(C)

FIGURE 12 (A) An optimized layout considering the first 50 eigenvalues (left: design variable distribution and right: 3d plot), (B) the 22th eigenvector, and (C) the distributions of the eigenvalues.

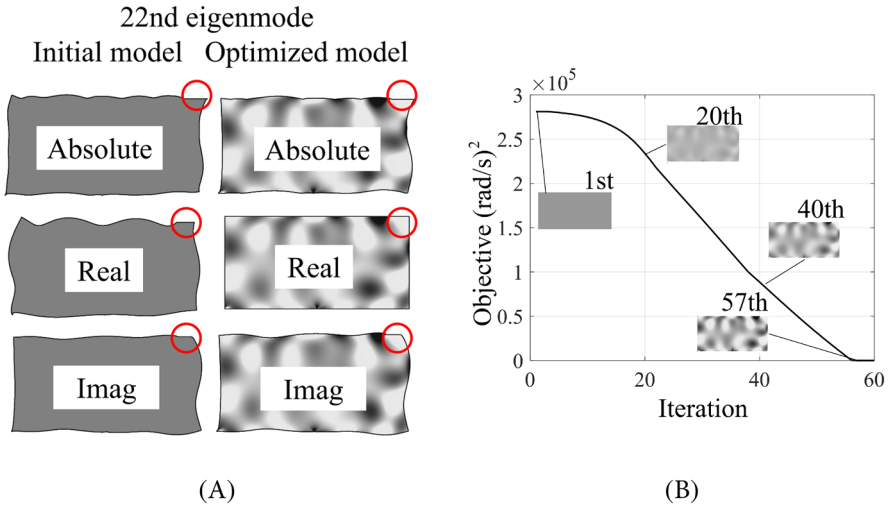

FIGURE 13 (A) The right eigenmode shape of the 22nd eigenmode (the eigenvectors near the brake are marked by the red circles) and (B) the optimization history of sum for square real eigenvalue.

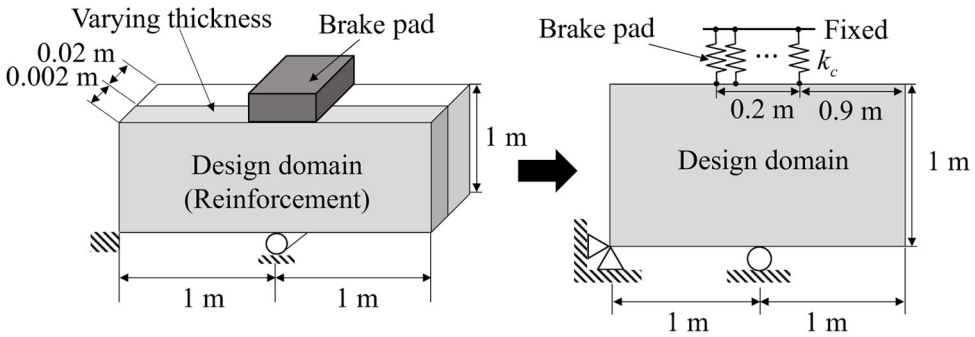

(A)

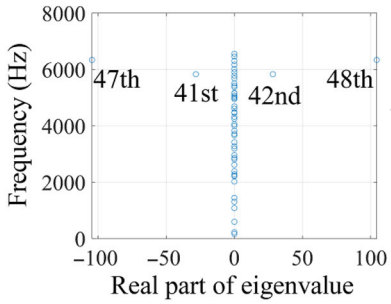

Complex eigenvalue with nonzero real part

	Real (λ_i) (rad/s)	Imag (λ_i) (rad/s) / Frequency (Hz)
41	−28.244 (rad/s)	36,651 (rad/s) / 5833.2 (Hz)
42	28.244 (rad/s)	36,651 (rad/s) / 5833.2 (Hz)
47	−104.39 (rad/s)	39,825 (rad/s) / 6338.4 (Hz)
48	104.39 (rad/s)	39,825 (rad/s) / 6338.4 (Hz)

(B)

FIGURE 14 Example 2-2: (A) The problem of reinforcement with a center pad (the number of elements: 200 by 100, Young's modulus = 200 GPa, $\rho = 7800$ kg/m^3, $\nu = 0.3$, the mass and stiffness penalization factors = 1, the number of friction spring: 21, $\mu = 0.5$) and (B) the initial eigenvalues.

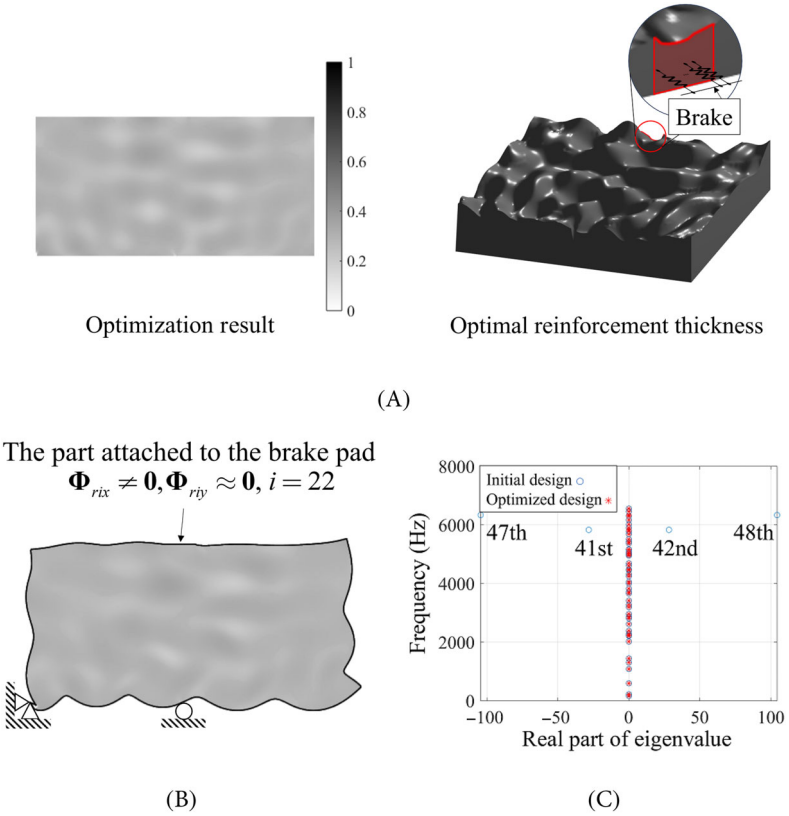

FIGURE 15 (A) An optimized layout with 50 eigenvalues (left: design variable distribution and right: 3d plot), (B) the 22th eigenvector, and (C) the distributions of the eigenvalues.

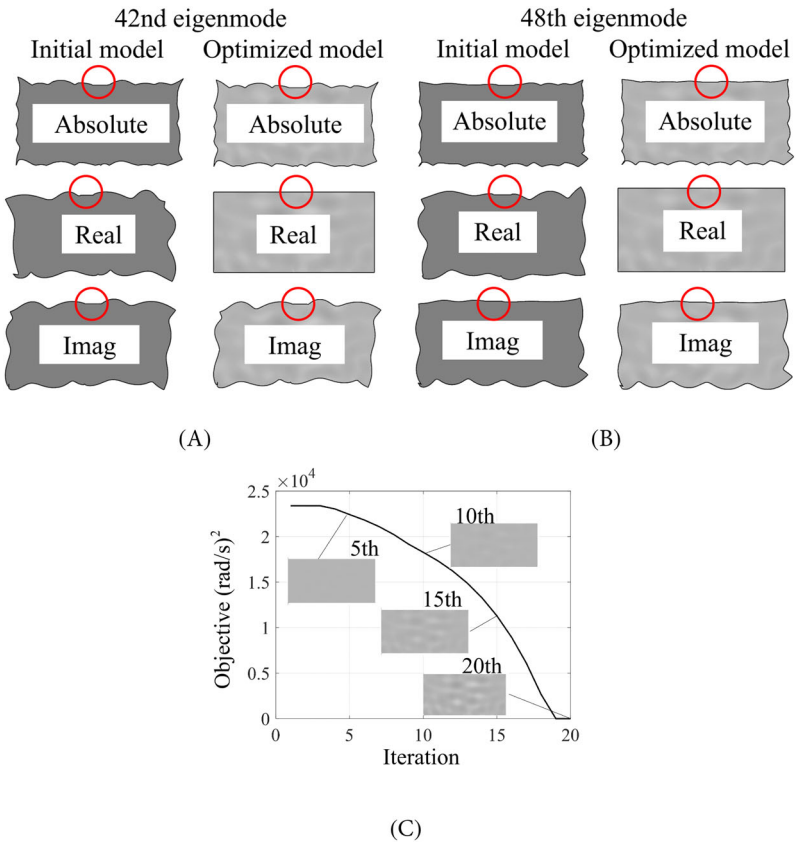

FIGURE 16 (A,B) The right eigen mode shapes of the 42nd and the 48th eigenmodes, respectively and (C) the optimization history.

4 | CONCLUSION

The present study develops a new topology optimization scheme considering dynamic stability, which causes squeal noise and significant structural vibration. Unlike a symmetric system, the left and right eigenvectors should be considered and computed for asymmetric system. In the theory of mechanical vibration, the real part of the complex eigenvalue causes the magnification of the vibration with respect to time or dynamic instability. To mitigate this side effect, the topology optimization scheme optimizing the reinforcement thickness is newly developed in the present study. Based on the numerical simulations and optimization results, the following can be observed. In the topology optimization, the complex responses of the eigenvalues due to the mode conversion and the mode switching make the topology optimization process difficult for the gradient-based optimizer. Therefore, spatially varying density variables are set to model the reinforcement thickness. By modeling the basic thickness and the reinforcement thickness, oscillations and highly nonlinear behaviors of the complex eigenvalues can be alleviated somewhat. However, even with the reinforcement thickness modeling at a 1/10 ratio of the basic thickness to the reinforcement thickness, the oscillations of the complex eigenvalues cannot be alleviated completely. Thus, the present research proposes using the summation of the complex eigenvalues as the objective function. The sum of the initial several complex eigenvalues can help mitigate the high oscillations associated with these eigenvalues. From our tests, the summation of the square of the approximately first 50 eigenvalues can be set as the objective function. The optimization results show that by designing the reinforcement structure, it tends to make the real parts of the eigenmode associated with the brake spring zero or near zero. This is reasonable, as the contribution of the brake spring can be minimized. In addition, it is also observed that the troublesome eigenmodes increase to a level at which they no longer significantly affect the objective function. In short, the present study develops a new topology optimization scheme for dynamic instability. For future research, the present scheme can be extended to consider advanced brake and contact models, and some experimental validations are also possible.

ACKNOWLEDGMENT

This work was supported by the National Research Foundation of Korea(NRF) grant funded by the Korea government(MSIT) (RS-2024-00351611).

CONFLICT OF INTERESTS STATEMENT

The author(s) declared no potential conflicts of interest with respect to the research, authorship, and/or publication of this article.

DATA AVAILABILITY STATEMENT

The datasets used and analyzed during the current study available from the corresponding author on reasonable request.

ORCID

Gil Ho Yoon https://orcid.org/0000-0002-0634-8329

REFERENCES

1. Kinkaid N, O'Reilly OM, Papadopoulos P. Automotive disc brake squeal. *J Sound Vib*. 2003;267(1):105-166.
2. Ouyang H, Nack W, Yuan Y, Chen F. Numerical analysis of automotive disc brake squeal: a review. *Int J Veh Noise Vib*. 2005;1(3–4):207-231.
3. Kang J. Squeal analysis of gyroscopic disc brake system based on finite element method. *Int J Mech Sci*. 2009;51(4):284-294.
4. Brunel J-F, Dufrénoy P, Naït M, Muñoz J-L, Demilly F. Transient models for curve squeal noise. *J Sound Vib*. 2006; 293(3–5):758-765.
5. Oberst S, Lai J. Nonlinear transient and chaotic interactions in disc brake squeal. *J Sound Vib*. 2015;342:272-289.
6. Wang X, Mo J, Ouyang H, et al. Squeal noise of friction material with groove-textured surface: an experimental and numerical analysis. *J Tribol*. 2016;138(2):021401.
7. Kang J, Krousgrill CM, Sadeghi F. Comprehensive stability analysis of disc brake vibrations including gyroscopic, negative friction slope and mode-coupling mechanisms. *J Sound Vib*. 2009;324(1–2):387-407.
8. Hochlenert D. Nonlinear stability analysis of a disk brake model. *Non Dyn*. 2009;58:63-73.
9. Du Y, Wang Y. Squeal analysis of a modal-parameter-based rotating disc brake model. *Int J Mech Sci*. 2017;131:1049-1060.

10. Nouby M, Mathivanan D, Srinivasan K. A combined approach of complex eigenvalue analysis and design of experiments (doe) to study disc brake squeal. *Int J Eng Sci Technol*. 2009;1(1):254-271.
11. Liu P, Zheng H, Cai C, et al. Analysis of disc brake squeal using the complex eigenvalue method. *Appl Acoust*. 2007; 68(6):603-615.
12. Kang J. Finite element modelling for the investigation of in-plane modes and damping shims in disc brake squeal. *J Sound Vib*. 2012;331(9):2190-2202.
13. Ding B, Squicciarini G, Thompson D. Effect of rail dynamics on curve squeal under constant friction conditions. *J Sound Vib*. 2019;442:183-199.
14. Junior MT, Gerges SN, Jordan R. Analysis of brake squeal noise using the finite element method: A parametric study. *Appl Acoust*. 2008;69(2):147-162.
15. Antunes DS, Masotti D, Ferreira NF, Neis PD, Miguel LF, Favero J. Damping effect on nonlinear drum brake squeal prediction. *J Braz Soc Mech Sci Eng*. 2022;44(3):97.
16. Hervé B, Sinou J-J, Mahé H, Jezequel L. Analysis of squeal noise and mode coupling instabilities including damping and gyroscopic effects. *Eur J Mech A Solid*. 2008;27(2):141-160.
17. Ghorbel A, Zghal B, Abdennadher M, Walha L, Haddar M. Investigation of friction-induced vibration in a disk brake model, including mode-coupling and gyroscopic mechanisms. *Proc Inst Mech Eng Pt D J Automob Eng*. 2020;234(2–3):887-896.
18. Kang J. Theoretical model of ball joint squeak. *J Sound Vib*. 2011;330(22):5490-5499.
19. Goto Y, Saomoto H, Sugiura N, Matsushima T, Ito S, Fukui A. *Structural Design Technology for Brake Squeal Reduction Using Sensitivity Analysis*. SAE Technical Paper 2010 Report 0148-7191.
20. Shintani K, Azegami H. Shape optimization for suppressing brake squeal. *Struct Multidisc Optim*. 2014;50:1127-1135.
21. Yoon J, Park J, Min S. Optimal disc brake design for reducing squeal instability using slip-dependent complex eigenvalue analysis. *Mech Syst Sig Proc*. 2022;177:109240.
22. Yoon GH, Donoso A, Carlos Bellido J, Ruiz D. Highly efficient general method for sensitivity analysis of eigenvectors with repeated eigenvalues without passing through adjacent eigenvectors. *Int J Numer Methods Eng*. 2020;121(20):4473-4492.
23. Pedersen NL. Maximization of eigenvalues using topology optimization. *Struct Multidisc Optim*. 2000;20:2-11.
24. Nilman J. *Modeling and Simulation of Brake Squeal in Disc Brake Assembly*. 2018.
25. Kang J. Finite element modeling for stick-slip pattern of squeal modes in disc brake. *J Mech Sci Technol*. 2014;28:4021-4026.
26. Denimal E, Sinou J-J, Nacivet S. Influence of structural modifications of automotive brake systems for squeal events with kriging meta-modelling method. *J Sound Vib*. 2019;463:114938.
27. Cantone F, Massi F. A numerical investigation into the squeal instability: Effect of damping. *Mech Syst Sig Proc*. 2011; 25(5):1727-1737.
28. Fritz G, Sinou J-J, Duffal J-M, Jézéquel L. Investigation of the relationship between damping and mode-coupling patterns in case of brake squeal. *J Sound Vib*. 2007;307(3–5):591-609.
29. Huang J, Krousgrill CM, Bajaj AK. Modeling of automotive drum brakes for squeal and parameter sensitivity analysis. *J Sound Vib*. 2006;289(1–2):245-263.
30. Ghazaly NM, Faris WF. Optimal design of a brake pad for squeal noise reduction using response surface methodology. *Int J Veh Noise Vib*. 2012;8(2):125-135.
31. Brunetti J, Massi F, Baillet L, et al. Application of the modal absorption index (mai) to reduce the cea instability over-prediction on a complex frictional system. *Proceedings of the ISMA*. ISMA; 2016.
32. Khuntiptong A, Chantalakhana C. Stability improvement of brake disc to mode coupling at high frequency squeal. *Appl Sci Eng Prog*. 2022;15(1):1-11.
33. Svanberg K. The method of moving asymptotes—a new method for structural optimization. *Int J Numer Methods Eng*. 1987; 24(2):359-373.

How to cite this article: Han SJ, Yoon GH. Reinforcement topology optimization considering the dynamic instability. *Int J Numer Methods Eng*. 2025;126(1):e7600. doi: 10.1002/nme.7600

APPENDIX A

A.1 Mesh refinement

For the stable analysis and optimization, the convergence of the complex eigenvalues should be guaranteed. To investigate the effect and the convergence of the complex eigenvalue, the presented complex eigenfrequency analysis of the following structure is carried out with the different meshes in Figure A1. As shown, the mesh refinement is important to ensure the accuracy of the eigenfrequency analysis.

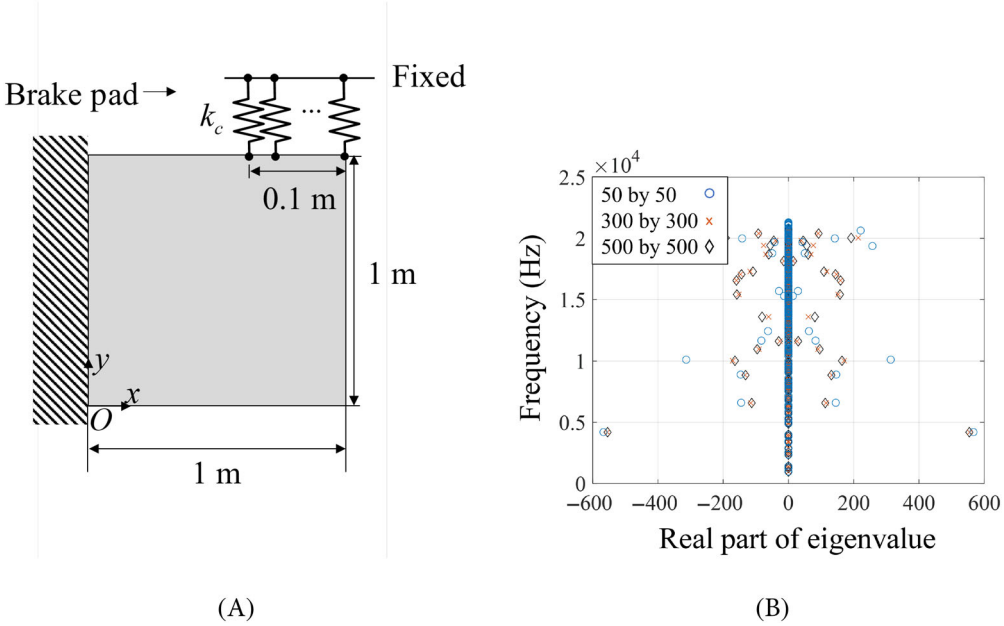

FIGURE A1 The mesh refinement test. (A) A model and (B) the results with the three different meshes.

A.2 Reinforcement design for mode conversion and mode coupling

To demonstrate the mode conversion and the coupling in topology optimization with void and solid, the illustrative structure with two by 2 plane stress element in Figure A2A can be considered. Only one spring simulating brake is attached to the right-top node. To investigate the mode conversion and the highly nonlinear behaviors of the complex eigenvalues, the behaviors of the 9th and 10th eigenvalues are investigated. As shown in Figure A2B,C, the behaviors become complex. Figure A2B plots the mode coupling and conversion of the 9th and 10th eigenvalues by varying the friction coefficient from 0 to 0.6. Around 0.46 for the friction coefficient, the two modes become coupled and the real parts of the two eigenvalues are separated. Thus, the system becomes unstable due to the 10th eigenvector. Figure A2C shows the behaviors of the eigenvalues of the system by varying the first density from zero to one. Figure A2C shows the curves of the eigenmodes with respect to the design variable and the real parts of the complex eigenvalues. This complexity becomes serious with a complicated configuration, that is, complex geometry and more elements. It is our opinion that this complex nonlinear behaviors make us impossible to solve the topology optimization with void and solid based on a gradient-based optimizer. Therefore, the considered topology optimization can be reformulated with the reinforcement concept.

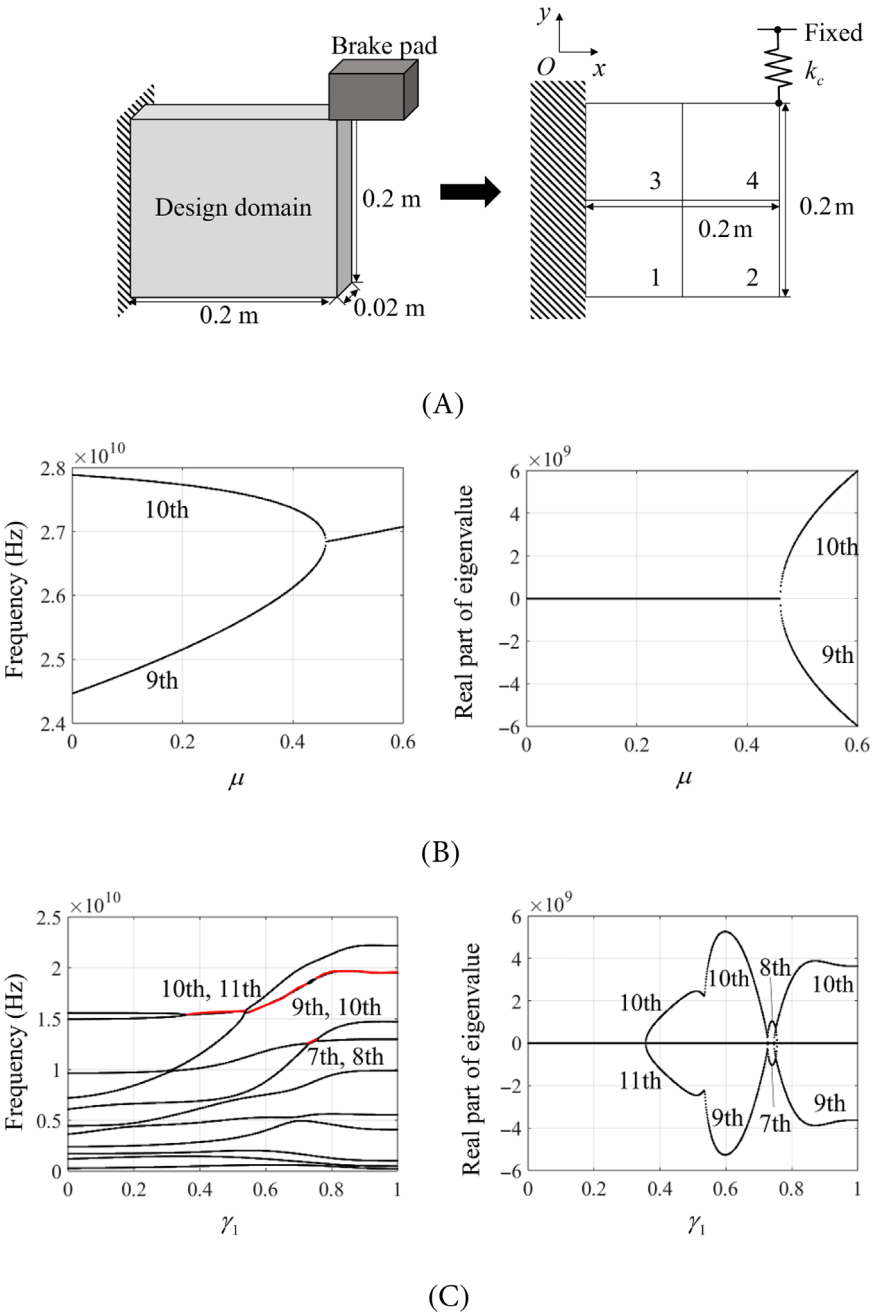

FIGURE A2 An element two by two quad example. (A) The problem with 4 quad elements (Young's modulus = 200 GPa, $\rho = 7800$ kg/m^3, $\nu = 0.3$, $k_c = 10^{14}$ N/m, $\mu = 0.5$, mass penalization=4, stiffness penalization=3, initial density = 0.3), (B) the mode coupling with the various friction coefficient and (C) the mode coupling with the various density of the first element.